Liner behaviour in an annular duct with swirling and sheared mean flow

Vianney Masson[*]
Département de Génie Mécanique, Université de Sherbrooke
Sherbrooke, QC, J1K2R1, Canada

James R. Mathews[†]
University of Cambridge
Cambridge, CB3 0WA, UK

Marlène Sanjose[‡], Stéphane Moreau[§]
Département de Génie Mécanique, Université de Sherbrooke
Sherbrooke, QC, J1K2R1, Canada

Hélène Posson[¶]
Airbus Commercial Aircraft
316 route de Bayonne, 31060 Toulouse cedex 09

The present study aims at addressing the effect of a swirling and sheared mean flow on the behavior of the liners in an annular duct. When the swirl is non zero in the vicinity of the wall, it is shown that the classical Myers boundary condition is no longer the correct limit for infinitely thin boundary layers. Indeed, centrifugal effects must be considered in the boundary condition. The acoustic transmission of a finite lined section in a infinite rigid annular duct is also assessed. In the presence of swirl, the classical mode matching conservation laws do not reduce to the conservation of fluctuating pressure and axial velocity. A new method of projection based on Chebyshev polynomials properties is proposed to address the physical problem. The swirl is shown to have a significant effect on the liner absorption.

[*]PhD candidate, Université de Sherbrooke, vianney.masson@usherbrooke.ca
[†]Research Associate, Department of Engineering, jrm214@cam.ac.uk
[‡]Assistant researcher, Université de Sherbrooke
[§]Professor, Université de Sherbrooke, AIAA Lifetime Member
[¶]Research engineer, Airbus Acoustic Department

Introduction

Next generations of turbofan, such as ultra-high bypass ratio (UHBR) engines, involve larger diameters. The inlet and exhaust will be shortened to balance the weight increase. Consequently, the relative importance of the acoustic treatments placed between the fan and the outlet guide vane will rise. This region is characterized by a strong swirling component, which can be of a similar amplitude to the axial velocity. Understanding the behavior of the liners in a swirling environment then becomes an important challenge to design quieter engines. Most of the time, they consist of locally reacting liners, typically made of a resistive layer placed over a honeycomb network which wraps the inner walls of the nacelle. Setting the physical properties of the panel and the length of the honeycomb cells defines the acoustic behavior of the devices. Mathematically, this response is characterized by the impedance of the liner Z, which links the acoustic pressure fluctuations p to the velocity fluctuations $\mathbf{v}$ through the relationship:

$$p = Z\mathbf{v} \cdot \mathbf{n} \tag{1}$$

at the surface of the liner, when the mean flow velocity is zero at the interface. In this definition, $\mathbf{n}$ represents the unit normal vector to the liner surface, pointing out of the flow. If the viscosity of the flow is neglected, the acoustic waves propagate in an Eulerian flow and the flow velocity at the wall can be theoretically non-zero. In that case, Eq. (1) no longer holds and a new boundary condition needs to be defined. After considerable debate in the 1970s, it has been finally accepted that continuity of normal acoustic displacement between the solid boundary and the fluid should be assumed.[1,2] Later on, Myers[3] extended this boundary condition to any surface shape. The so-developed Ingard-Myers boundary condition, also referred to as Myers boundary condition, has been considered as the reference since then, for more than thirty years.

More recently, limits of Ingard-Myers boundary condition have been demonstrated, either mathematically[4] or experimentally.[5] Modified Myers boundary conditions have been developed to regularize its mathematical formulation by including the effect of a boundary layer to first order[6,7] or to correct its non-physical behavior by considering the viscosity in the formulation.[5] Gabard[8] summarized the modified models that consider a boundary layer and showed both the limitations of Myers boundary condition and the accuracy of Brambley's boundary condition in acoustic transmission with liners. Lately, Khamis & Brambley[9] extended Brambley's model by including the effect of the boundary layer to second order, and thereby improving the accuracy of the model.

Besides, Guan *et al.*[10] studied the effect of swirl on the acoustic transmission in a lined annular duct. They coupled a normal-mode analysis with a mode-matching method to compute the absorption of a lined section. More recently, Posson & Peake[11] developed an acoustic analogy for an arbitrary swirling and sheared flow in an annular duct. They extended it to the presence of acoustic treatments on the surface of the duct, and applied their approach to compute the trailing-edge noise of the rotor.[12] Mathews & Peake[13] proposed an asymptotic extension of Posson & Peake in the high-frequency range. Using a finite element method to compute the eigenvalues and eigenfunctions, Maldonado *et al.*[14] also studied the sound transmission in a lined annular duct with swirl. All these authors considered Myers boundary condition in their approach.

The aim of the present paper is to study the behavior of liners in an annular duct with swirling and sheared flow. Notably, the importance of the boundary condition used at the interface will be assessed by considering alternatives to the Ingard-Myers boundary. Particularly, it will be shown that Myers boundary condition is incorrect as the limit of an infinitely thin boundary layer in the presence of swirl and that centrifugal effect should be considered in the equivalent boundary condition. Boundary conditions which assume the presence of a boundary layer will also be considered. The present work can be seen as an extension of Guan's work[10] to an arbitrary flow, and to a more accurate boundary condition. It can also be seen as an extension of Gabard's study[8] on liners boundary conditions to a swirling and sheared mean flow.

The corrected Myers boundary condition will be presented in section II. The different boundary conditions as well as the eigenvalue formulation used to determine the modal content will be presented in section III. A mode-matching formalism based on the conservation of the mass flow and the total enthalpy is developed to deal with the absorption of a duct-lined section in presence of a swirling and sheared mean flow. Due to the nature of the eigenfunctions, a specific projection method is used. The method is detailed in section V. Finally, first conclusions about the effect of the swirl on the acoustic transmission with the new boundary condition are drawn in section VI.

I. Governing equations

The evolution of acoustic perturbations inside an inviscid compressible perfect gas is considered in an infinite annular duct with acoustic treatments both on the inner and the outer surfaces. The surface impedances of the outer wall liners are Z_h^* and Z_1^* respectively. They are located at the radii R_h^* and R_t^* respectively, $h = R_h^*/R_t^*$ being the hub-to-tip ration. The mid-span radius is defined by $R_m^* = (R_h^* + R_t^*)/2$. The duct section does not vary in the axial direction. Lengths, speeds and density are made non-dimensional by R_t^*, $c_0^*(R_m^*)$ and $\rho_0^*(R_m^*)$ respectively, and other variables by the relevant combination of these values. The radial component of the mean flow is assumed to be zero and the axial and azimuthal components U_x and U_θ may vary along the radius, leading to the following definition of the mean velocity field:

$$\mathbf{U}(r) = (0, U_\theta(r), U_x(r)). \tag{2}$$

The mean flow is assumed homentropic, which means that the mean flow entropy is constant everywhere in the fluid domain. Thus, the mean density and the mean speed of sound may vary radially according to the relationships:

$$c_0^2(r) = 1 + (\gamma - 1)\int_{R_m}^{1} \frac{U_\theta(r')}{r'}\mathrm{d}r', \tag{3}$$

$$\rho_0(r) = \left[c_0^2(r)\right]^{1/(\gamma-1)}, \tag{4}$$

where γ is the ratio of specific heat capacities. Every flow variable (referred to as the subscript "to") are decomposed into a sum of a mean and a fluctuating part so that:

$$\mathbf{U}_{to} = \mathbf{U} + \mathbf{u}, \quad \rho_{to} = \rho_0 + \rho, \quad P_{to} = P_0 + p. \tag{5}$$

Here, $\mathbf{u} = (u, v, w)$ is the fluctuating velocity, p and ρ are the fluctuating pressure and density respectively. The Navier-Stokes equations linearized with respect to the mean flow defined in Eq. (2) reduce to:

$$\frac{1}{c_0^2}\frac{\mathrm{D}_0 p}{\mathrm{D}t} + u\frac{\mathrm{d}\rho_0}{\mathrm{d}r} + \rho_0 \mathrm{div}(\mathbf{u}) = 0, \tag{6}$$

$$\rho_0\left[\frac{\mathrm{D}_0 u}{\mathrm{D}t} - 2\frac{U_\theta v}{r}\right] - \frac{U_\theta^2}{r c_0^2}p + \frac{\partial p}{\partial r} = 0, \tag{7}$$

$$\rho_0\left[\frac{\mathrm{D}_0 v}{\mathrm{D}t} + \frac{u}{r}\frac{\partial (rU_\theta)}{\partial r}\right] + \frac{1}{r}\frac{\partial p}{\partial \theta} = 0, \tag{8}$$

$$\rho_0\left[\frac{\mathrm{D}_0 w}{\mathrm{D}t} + u\frac{\partial U_x}{\partial r}\right] + \frac{\partial p}{\partial x} = 0, \tag{9}$$

where $\mathrm{D}_0/\mathrm{D}t$ is the convective operator with respect to the mean flow. The pressure and velocity disturbances are Fourier-transformed with respect to the time t and the axial coordinate x. Besides, the azimuthal periodicity of the physical statement allows decomposing the perturbation field as a Fourier series along the θ coordinate, such as every acoustic variable can be written:

$$\varphi(r, x, t) = \int_\omega \sum_m \int_k \widehat{\varphi}(r) e^{\mathrm{i}(kx + m\theta - \omega t)}\mathrm{d}k\mathrm{d}\omega.$$

where $\widehat{\varphi}$ is the Fourier transform of φ (φ standing for p, u, v or w), ω is the frequency, k is the axial wavenumber and m is the azimuthal mode order. Given $\Lambda = kU_x + mU_\theta/r - \omega$, the linear governing equations in the spectral domain reads:

$$\mathrm{i}\frac{\Lambda}{c_0^2}\hat{p} = -\frac{\mathrm{d}\rho_0}{\mathrm{d}r}\hat{u} - \frac{\rho_0}{r}\frac{\mathrm{d}(r\hat{u})}{\mathrm{d}r} - \mathrm{i}\frac{\rho_0 m}{r}\hat{v} - \mathrm{i}k\rho_0\hat{w}, \tag{10}$$

$$\mathrm{i}\rho_0\Lambda\hat{u} = 2\frac{\rho_0 U_\theta}{r}\hat{v} + \frac{U_\theta^2}{rc_0^2}\hat{p} - \frac{\mathrm{d}\hat{p}}{\mathrm{d}r}, \tag{11}$$

$$\mathrm{i}\rho_0\Lambda\hat{v} = -\frac{\rho_0}{r}\frac{\partial(rU_\theta)}{\partial r}\hat{u} - \frac{\mathrm{i}m}{r}\hat{p}, \tag{12}$$

$$\mathrm{i}\rho_0\Lambda\hat{w} = -\rho_0\frac{\partial U_x}{\partial r}\hat{u} - \mathrm{i}k\hat{p}. \tag{13}$$

Assuming the radial equilibrium of the mean flow, the latter equations can be combined to yield a system of two coupled first-order differential equations on the pressure $\hat{p}$ and the radial fluctuating velocity $\hat{u}$ only, given by

$$\frac{\mathrm{d}\hat{u}}{\mathrm{d}r} + \left[\frac{1}{r} + \frac{U_\theta^2(r)}{rc_0^2(r)} - \frac{k}{\Lambda(r)}\frac{\mathrm{d}U_x(r)}{\mathrm{d}r} - \frac{m}{\Lambda(r)r^2}\frac{\mathrm{d}}{\mathrm{d}r}\left(rU_\theta(r)\right)\right]\hat{u} + \mathrm{i}\frac{1}{\rho_0(r)\Lambda(r)}\left(\frac{\Lambda^2(r)}{c_0^2(r)} - \frac{m^2}{r^2} - k^2\right)\hat{p} = 0, \tag{14}$$

which may be written equivalently:

$$\frac{\mathrm{d}}{\mathrm{d}r}\left(\frac{r\hat{u}}{\Lambda(r)}\right) - \frac{1}{\Lambda(r)}\left(\frac{2mU_\theta(r)}{r\Lambda(r)} - \frac{U_\theta^2(r)}{c_0^2(r)}\right)\hat{u} = -\mathrm{i}\frac{r}{\rho_0(r)\Lambda^2(r)}\left(\frac{\Lambda^2(r)}{c_0^2(r)} - \frac{m^2}{r^2} - k^2\right)\hat{p}. \tag{15}$$

For the pressure, the radial-momentum linear equation is rewritten:

$$\frac{\mathrm{d}\hat{p}}{\mathrm{d}r} + \left(\frac{2mU_\theta(r)}{\Lambda(r)r^2} - \frac{U_\theta^2(r)}{rc_0^2(r)}\right)\hat{p} = -\mathrm{i}\frac{\rho_0(r)}{\Lambda(r)}\left(\Lambda^2(r) - \frac{2U_\theta(r)}{r^2}\frac{\mathrm{d}}{\mathrm{d}r}\left(rU_\theta(r)\right)\right)\hat{u}. \tag{16}$$

Eqs. (14) and (16) are the equivalent of Eqs. (A4) and (A7) in the appendices of Posson & Peake[11] in the frequency domain. They are also the extension of Khamis & Brambley equations[9] (2.10) to a swirling flow. They will be used to establish the corrected Myers boundary condition.

II. Correction of Myers' boundary condition in presence of a swirling flow

A. Classical Myers' boundary condition

Assuming the continuity of the acoustic normal displacement through an infinitely thin boundary layer leads to the classical Myers boundary condition.[3] It reads with the present conventions:

$$\hat{u}(h) = \frac{kU_x + mU_\theta/r - \omega}{\omega Z_h}\hat{p}(h), \quad \text{and} \quad \hat{u}(1) = -\frac{kU_x + mU_\theta/r - \omega}{\omega Z_1}\hat{p}(1) \tag{17}$$

at hub and at tip respectively. In the following, it will be shown that when the mean flow is swirling, Eq. (17) is not the correct limit when the boundary layer thickness tends to zero in presence of swirl.

B. Assumptions

The aim of this section is to substitute the effect of a boundary layer with the boundary condition in (1) by an equivalent boundary condition in a flow where the boundary layer is not taken into account. In order to address such a problem, Eversman & Beckemeyer[2] proposed an approach based on an asymptotic matching between an inner solution in the boundary layer and an outer solution outside the boundary layer, which would exist if there was no boundary layer. This method has been reused by several authors such as Myers & Chuang,[15] Brambley[6] and Khamis & Brambley[9] for an axial flow. We propose to extend it to the case of a swirling flow. In order to develop the asymptotic expansion, the distance to the wall y is introduced. As in Brambley,[6] it is scaled by the boundary layer thickness δ such that $r = 1 - \delta y$ at the outer wall and $r = h + \delta y$ at the inner wall, with $\delta \ll 1$. Let $U_x^{\mathrm{nbl}}(r)$ and $U_\theta^{\mathrm{nbl}}(r)$ the flow velocity profiles without the boundary layer. The variations of the mean flow velocities verify:

$$\frac{\mathrm{d}U_x^{\mathrm{nbl}}}{\mathrm{d}r} \sim \frac{U_x^{\mathrm{nbl}}(1)}{h}, \qquad \frac{\mathrm{d}U_\theta^{\mathrm{nbl}}}{\mathrm{d}r} \sim \frac{U_\theta^{\mathrm{nbl}}(1)}{h}$$

in the core flow, where h is in the order of unity, and

$$\frac{\mathrm{d}U_x}{\mathrm{d}y} \sim \frac{U_x^{\mathrm{nbl}}(1)}{\delta}, \qquad \frac{\mathrm{d}U_\theta}{\mathrm{d}y} \sim \frac{U_\theta^{\mathrm{nbl}}(1)}{\delta}$$

in the boundary layer. It follows that

$$\frac{\mathrm{d}U_x^{\mathrm{nbl}}}{\mathrm{d}r} \ll \frac{\mathrm{d}U_x}{\mathrm{d}y}, \qquad \frac{\mathrm{d}U_\theta^{\mathrm{nbl}}}{\mathrm{d}r} \ll \frac{\mathrm{d}U_\theta}{\mathrm{d}y}.$$

Since the present approach is based on an asymptotic matching on the inner variable y, the outer variables can be assumed constant in the frame of the present analysis. They will be taken as their value in $r = 1$, such as:

$$U_x^{\mathrm{nbl}}(r) = U_x^{\mathrm{nbl}}(1) = M_{x,1},$$
$$U_\theta^{\mathrm{nbl}}(r) = U_\theta^{\mathrm{nbl}}(1) = M_{\theta,1},$$

in the vicinity of the outer wall, and as their value in $r = h$

$$U_x^{\mathrm{nbl}}(r) = U_x^{\mathrm{nbl}}(h) = M_{x,h},$$
$$U_\theta^{\mathrm{nbl}}(r) = U_\theta^{\mathrm{nbl}}(h) = M_{\theta,h},$$

near the inner wall. Firstly, a constant flow velocity profile is assumed through the duct section so that $M_{x,h} = M_{x,1} = M_x$, and $M_{\theta,h} = M_{\theta,1} = M_\theta$. Taking constant mean velocities forces the profiles of the speed of sound and the mean density, from Eqs. (3) and (4) to be defined by:

$$\left(c_0^{\mathrm{nbl}}(r)\right)^2 = 1 + 0.4 M_\theta \left[\log(r) - \log(R_m)\right], \tag{18}$$

and

$$\rho_0^{\mathrm{nbl}}(r) = \left(1 + 0.4 M_\theta \left[\log(r) - \log(R_m)\right]\right)^{5/2}. \tag{19}$$

C. Derivation of the corrected boundary condition at the outer wall

The boundary condition is developed at the outer wall first.

1. *Outer solution*

The outer solution corresponds to the fluctuations propagating in the outer flow. It is obtained by writing a Taylor expansion of $\hat{u}$ and $\hat{p}$ in the vicinity of the outer wall. At leading order, it reads :

$$\hat{u}_o(1 - \delta y) = \hat{u}_o(1) + O(\delta), \tag{20}$$
$$\hat{p}_o(1 - \delta y) = \hat{p}_o(1) + O(\delta), \tag{21}$$

where the subscript "o" stands for the outer solution. The eigenfunctions $\hat{p}_o$ and $\hat{u}_o$ represent the pressure and the radial velocity respectively if the boundary layer does not exist. Even if there is no analytic expression for them, they can be determined by a pseudo-spectral method for example, as done in section III. They are assumed to be known, in particular $\hat{p}_\infty^1$ and $\hat{u}_\infty^1$ are introduced such as,

$$\hat{p}_o(1) = \hat{p}_\infty^1, \quad \hat{u}_o(1) = \hat{u}_\infty^1.$$

In the following, the inner solution for $\hat{p}$ and $\hat{v}$ will be matched to Eqs. (20) and (21)

2. *Inner solutions*

To compute the inner solution, Eqs. (15) and (16) are expanded by replacing r by $1 - \delta y$ [a] . To leading order, Eq. (16) becomes

[a] It is also possible to start the matching method from Eqs. (10)-(13), as done in Mathews *et al.*[16]

$$\hat{p}_y(y) = \frac{2\mathrm{i}\rho_0 U_\theta U_{\theta,y}}{kU_x + mU_\theta - \omega}\hat{u}(y) + O(\delta). \tag{22}$$

where the y-dependence has been kept implicitly. The subscript "$_y$" represents the derivative with respect to y and for every variable Φ; $\Phi(y)$ improperly stands for $\Phi(r = 1 - \delta y)$. Similarly, Eq. (15) is rewritten in terms of the inner variable y

$$\left(\frac{\hat{u}(y)}{kU_x + mU_\theta - \omega}\right)_y = O(\delta). \tag{23}$$

The solution to these equations must be determined to be matched with the outer solution. The acoustic pressure and normal velocity are expanded in the following way:

$$\hat{p}(y) = \hat{p}_0(y) + O(\delta), \tag{24}$$
$$\hat{u}(y) = \hat{u}_0(y) + O(\delta). \tag{25}$$

The form of Eq. (23) allows determining $\hat{u}_0$. At zeroth order, it reduces to:

$$\left(\frac{\hat{u}_0(y)}{kU_x(y) + mU_\theta(y) - \omega}\right)_y = 0.$$

Then, by posing $\Lambda_0(y) = kU_x(y) + mU_\theta(y) - \omega$,

$$\hat{u}_0(y) = \beta_0 \Lambda_0(y). \tag{26}$$

Similarly, only leading order terms in δ are kept in Eq. (22). This reads:

$$\hat{p}_{0,y}(y) = \frac{2\mathrm{i}\rho_0 U_\theta(y) U_{\theta,y}(y)}{\Lambda_0(y)}\hat{u}_0(y),$$

then

$$\hat{p}_0(y) = A_0 + \mathrm{i}\beta_0 \int_0^y \rho_0(y') \left(U_\theta^2(y')\right)_y \mathrm{d}y' \tag{27}$$

The integral over y' is bounded since $U_{\theta,y}(y) = M_{\theta,y} = 0$ outside the boundary layer according to section II.B. The constants β_0 and A_0 can be determined by matching the leading order inner solutions with the outer ones.

3. Matching

Matching Eq. (26) with the outer solution (Eq. (21)) for large y gives the value of the constant β_0:

$$\beta_0 = \frac{\hat{u}^1_\infty}{\Lambda^1_\infty}, \tag{28}$$

where $\Lambda^1_\infty = kM_{x,1} + mM_{\theta,1} - \omega$ has been defined for conciseness. Matching $\hat{p}_0$ with leading order terms of $\hat{p}_o$ in Eq. (20) for large y gives:

$$A_0 = \hat{p}^1_\infty - \frac{\mathrm{i}\hat{u}^1_\infty I_0}{\Lambda^1_\infty}, \tag{29}$$

where

$$I_0 = \int_0^\infty \rho_0(y) \left(U_\theta^2(y)\right)_y \mathrm{d}y. \tag{30}$$

4. Boundary condition

At $r = 1$, the surface impedance of the liner at the outer wall is defined by $Z_1 = \hat{p}(1)/\hat{v}(1)$. As in Khamis & Brambley,[9] the boundary condition is expressed as an equivalent impedance relating $\hat{u}^1_\infty$ and p^1_∞. At leading order, it reads:

$$Z_{\text{eff}}(1) = \frac{\hat{p}^1_\infty}{\hat{u}^1_\infty} = -\frac{\omega}{\Lambda^1_\infty}\left(Z_1 + \frac{\mathrm{i}}{\omega}\int_{R_m}^1 \rho_0 \frac{\mathrm{d}}{\mathrm{d}r}\left(U_\theta^2\right)\mathrm{d}r\right). \tag{31}$$

The right-hand side term inside the parentheses does not appear in the classical Myers boundary condition (see Eq. (17)). It is due to the centrifugal effect acting on the liner. When the mean swirl is zero, the latter term reduces to zero and Eq. (31) reduces to Myers' boundary condition for an axial mean flow. Eq. (31) is the correct boundary condition for a vanishing boundary layer in presence of a swirling flow. In Mathews *et al.*,[16] the method is extended to first order.

D. Extension to the inner wall

At the inner wall, the surface impedance is defined by $Z_h = -\hat{p}(h)/\hat{v}(h)$. Applying the same method leads to the corrected Myers boundary condition:

$$Z_{\text{eff}}(h) = -\frac{\hat{p}^h_\infty}{\hat{u}^h_\infty} = -\frac{\omega}{\Lambda^h_\infty}\left(Z_h + \frac{\mathrm{i}}{h\omega}\int_h^{R_m} \rho_0 \frac{\mathrm{d}}{\mathrm{d}r}\left(U_\theta^2\right)\mathrm{d}r\right), \tag{32}$$

where $\hat{p}^h_\infty = \hat{p}_o(h)$, $\hat{u}^h_\infty = \hat{u}_o(h)$, and $\Lambda^h_\infty = kM_{x,h} + mM_{\theta,h}/h - \omega$.

E. Extension to a varying outer mean flow away from the walls

The corrected Myers boundary condition has been developed previously for a constant axial velocity and for a constant swirl. It is suggested here to extend it to velocity profiles which may vary through the duct section. To do so, the parameters $\widehat{U_x}$ and $\widehat{U_\theta}$ are introduced such that

$$\widehat{U_x}(y) = \frac{U_x^{\text{nbl}}(0)U_x(y)}{U_x^{\text{nbl}}(y)} = U_x(y) + O(\delta), \tag{33}$$

and

$$\widehat{U_\theta}(y) = \frac{U_\theta^{\text{nbl}}(0)U_\theta(y)}{U_\theta^{\text{nbl}}(y)} = U_\theta(y) + O(\delta), \tag{34}$$

where U_x^{nbl} and U_θ^{nbl} now depend on y. Then, U_θ can be simply replaced by $\widehat{U_\theta}$ in Eqs. (22) and (23) since the equations are unchanged at leading order. Unlike U_x and U_θ, $\widehat{U_x}$ and $\widehat{U_\theta}$ have a well-defined limit as $y \to \infty$. In particular,

$$\widehat{U_\theta}(y) = U_\theta^{\text{nbl}}(0), \qquad \widehat{U_x}(y) = U_x^{\text{nbl}}(0), \qquad \forall y \geq 1,$$

and the integral I_0 remains bounded. Since $\widehat{U_x}(0) = U_x(0)$ and $\widehat{U_\theta}(0) = U_\theta(0)$, the boundary condition becomes:

$$Z_{\text{eff}}(h) = -\frac{\hat{p}^h_\infty}{\hat{u}^h_\infty} = -\frac{\omega}{\Lambda^h_\infty}\left(Z_h + \frac{\mathrm{i}}{h\omega}\int_h^{R_m} \rho_0 \frac{\mathrm{d}}{\mathrm{d}r}\left(\widehat{U_\theta}^2\right)\mathrm{d}r\right), \tag{35}$$

and

$$Z_{\text{eff}}(1) = \frac{\hat{p}^1_\infty}{\hat{u}^1_\infty} = -\frac{\omega}{\Lambda^1_\infty}\left(Z_1 + \frac{\mathrm{i}}{\omega}\int_{R_m}^1 \rho_0 \frac{\mathrm{d}}{\mathrm{d}r}\left(\widehat{U_\theta}^2\right)\mathrm{d}r\right). \tag{36}$$

F. Approximating the boundary condition

For thin boundary layers, the density hardly varies and the corrected boundary conditions can be approximated by:

$$Z^\ddagger_{\text{eff}}(h) = -\frac{\omega}{\Lambda^h_\infty}\left(Z_h + \frac{\mathrm{i}}{h\omega}\rho_0^{\text{nbl}}(h)M^2_{\theta,h}\right), \tag{37}$$

for the inner wall, and

$$Z^{\ddagger}_{\text{eff}}(1) = -\frac{\omega}{\Lambda^1_\infty}\left(Z_1 - \frac{\mathrm{i}}{\omega}\rho_0^{\text{nbl}}(1)M^2_{\theta,1}\right), \tag{38}$$

for the outer wall. This holds for both a constant flow and a varying flow presented in section II.E The relevance of this approximation will be discussed in section IV.A.

III. Eigenvalue formulation

In the wavenumber-frequency domain, it is possible to combine the governing equations (10) - (13) to set up an eigenvalue problem such that k is an eigenvalue and where the eigensolutions of the problem give the radial profile of the disturbance variables. It reads:

$$k\mathcal{B}\mathbf{X} = \mathcal{A}\mathbf{X}, \tag{39}$$

where $\mathbf{X} = (\hat{u}, \mathrm{i}\hat{v}, \mathrm{i}\hat{w}, \hat{p})^T$ is the eigenvector of the disturbances, with the superscript "^{T}" referring to the transpose of a matrix. $\mathcal{A}$ and $\mathcal{B}$ depends on the linearized governing equations and the boundary conditions. This eigenvalue problem is solved by means of a pseudo-spectral method applied on a Chebyshev colocation grid as suggested by Khorrami *et al.*[17] and performed by Posson & Peake[11] and Mathews & Peake.[13] At the lined walls, a boundary condition must be considered to close the problem. To the authors knowledge, all the in-duct transmission studies which consider both swirling flow and lined walls rely on Myers' boundary condition at the interface.[10,12,14] In this paper, Myers' boundary condition is compared with the leading-order corrected Myers boundary condition and with the application of the surface impedance definition for flows including a boundary layer. In the following, the boundary conditions are rewritten to fit with the eigenvalue formulation.

A. Classical Myers' boundary condition

Since Myers' boundary condition is k-linear, it can be easily included in the eigenvalue formulation (see Eq. (17)). This is what has been done so far in the literature.[10,12,14,18]

B. New Myers' boundary condition

The corrected Myers boundary condition is also k-linear whereas it is shown in Mathews *et al.*[16] that this is not true for the first-order modified boundary condition with swirl in general. The impedances $Z^{\ddagger}_h$ and $Z^{\ddagger}_1$ are introduced such that:

$$Z^{\ddagger}_h = Z_h + \frac{\mathrm{i}}{h\omega}\rho_0^{\text{nbl}}(h)M^2_{\theta,h}. \tag{40}$$

$$Z^{\ddagger}_1 = Z_1 - \frac{\mathrm{i}}{\omega}\rho_0^{\text{nbl}}(1)M^2_{\theta,1}. \tag{41}$$

Then, the modified Myers boundary condition to leading order reads:

$$\hat{u}(h) = \frac{kU_x(h) + mU_\theta(h)/h - \omega}{\omega Z^{\ddagger}_h}\hat{p}(h), \quad \text{and} \quad \hat{u}(1) = -\frac{kU_x(1) + mU_\theta(1) - \omega}{\omega Z^{\ddagger}_1}\hat{p}(1), \tag{42}$$

which is the same formulation as the classical Myers boundary condition, where the impedances have been replaced only.

C. Boundary layer treatment

In order to challenge the old Myers and the corrected Myers boundary conditions, a boundary layer profile can be included in the mean flow, such that the flow is zero at the interface. Given the outer flow (varying or not), the exponential envelope L_α is introduced such that

$$L_\alpha(r) = 1 - e^{-\alpha(r-h)} - e^{-\alpha(1-r)}. \tag{43}$$

The realistic profile is defined by multiplying the outer flow by L_α. The boundary layer thickness is controlled by the parameter α, with $\delta \propto 1/\alpha$. The displacement thickness is defined by:

$$\varepsilon_h = 2\int_h^{R_m}\left(1-\frac{U_x(r)}{U_x^{\mathrm{nbl}}(r)}\right)\mathrm{d}r, \qquad \varepsilon_1 = 2\int_{R_m}^{1}\left(1-\frac{U_x(r)}{U_x^{\mathrm{nbl}}(r)}\right), \tag{44}$$

at the inner wall and at the outer wall respectively. Gabard[8] applied several boundary layer profiles in the case of a non-swirling flow and showed that the shape of the boundary layer had a weak importance on the result. The same conclusion is expected for a swirling mean flow. However, the influence of the boundary layer shape will not be addressed in the frame of the present study. For a mean flow which includes a boundary layer, the boundary condition reduces to

$$\hat{p}(h) = -Z_h\hat{u}(h) \qquad \text{and} \qquad \hat{p}(1) = Z_1\hat{u}(1) \tag{45}$$

IV. Influence of the boundary condition on the acoustic propagation

A. Validation of the approximation for thin boundary layers

The approximated boundary condition introduced in section II.F is challenged here at the outer wall. To do so, $Z_1^\star$ can be introduced so that

$$Z_1^\star = Z_1 + \frac{\mathrm{i}}{\omega}\int_{R_m}^{1}\rho_0\frac{\mathrm{d}}{\mathrm{d}r}\left(U_\theta^2\right)\mathrm{d}r. \tag{46}$$

In order to validate the approximated form of the new Myers boundary condition, the values of $Z_1^\star$ and $Z_1^\ddagger$ are compared for different boundary layer thicknesses. The results are presented in Table 1 for $\omega = 5$, $U_\theta = 0.5$ and $Z_1 = 1 - 2\mathrm{i}$. The approximate solution gets closer to the reference when the boundary layer

α	100	200	300	600	1000	3000
$Z_1^\star$	$1-2.053597\mathrm{i}$	$1-2.053635\mathrm{i}$	$1-2.053648\mathrm{i}$	$1-2.053661\mathrm{i}$	$1-2.053666\mathrm{i}$	$1-2.053672\mathrm{i}$
$Z_1^\ddagger$	$1-2.053674\mathrm{i}$	$1-2.053674\mathrm{i}$	$1-2.053674\mathrm{i}$	$1-2.053674\mathrm{i}$	$1-2.053674\mathrm{i}$	$1-2.053674\mathrm{i}$

Table 1: Comparison of $Z^\ddagger$ and Z^* for different boundary layer thicknesses. The parameters used are $\omega = 5$, $U_\theta = 0.5$ and $Z_1 = 1 - 2\mathrm{i}$.

thickness tends to zero, as expected. For all the tested boundary layers, the results are the same up to three decimals. Because of this, the approximated form of the boundary condition will be used in the following.

B. Validation of the corrected Myers boundary condition

First, it is proposed to assess the corrected boundary condition on a simple case. The canonical case chosen for the study stands for a constant swirl and a constant axial flow such that $M_x = M_\theta = 0.5$. The duct section is characterized by the non-dimensional inner radius $h = 0.5$. The non-dimensional angular frequency $\omega = 4$ and the azimuthal mode order $m = -1$ are considered. The surface impedance at the inner and at the outer wall are defined by $Z_1 = Z_h = 1 - \mathrm{i}$. For this case, the approximated boundary condition gives $Z_h^\ddagger = 1.000 - 0.887\mathrm{i}$ and $Z_1^\ddagger = 1.000 - 1.067\mathrm{i}$. First, eigenvalues obtained with the old Myers and the new Myers boundary conditions are compared with the ones obtained with a realistic boundary layer, for several boundary layer thicknesses. As the boundary layer thickness tends to zero, the eigenmodes become harder to predict numerically when simulating the boundary layer. In table 2, the eigenvalues of the two most "cut-on" upstream and downstream modes are considered.

The additional centrifugal term in the corrected Myers boundary condition has an effect, since it differs from the classical Myers boundary condition from the second decimal in this case. Furthermore when the boundary layer thickness tends to zero, the eigenvalues indeed converge towards the new Myers boundary condition. This suggests that Eqs. (37) and (38) are the correct limit for a vanishing boundary layer.

α	300	1000	5000	Old Myers	Corrected Myers
ε	7×10^{-3}	2×10^{-3}	4×10^{-4}	0	0
D1	$2.3552 + 0.7498\mathrm{i}$	$2.3543 + 0.7498\mathrm{i}$	$2.3540 + 0.7498\mathrm{i}$	$2.3488 + 0.7436\mathrm{i}$	$2.3538 + 0.7499\mathrm{i}$
D2	$1.0537 + 5.3072\mathrm{i}$	$1.1232 + 5.3315\mathrm{i}$	$1.1481 + 5.3405\mathrm{i}$	$1.1067 + 5.3353\mathrm{i}$	$1.1548 + 5.3430\mathrm{i}$
U1	$-6.1198 - 1.4531\mathrm{i}$	$-6.1690 - 1.4476\mathrm{i}$	$-6.1856 - 1.4457\mathrm{i}$	$-6.2015 - 1.4159\mathrm{i}$	$-6.1890 - 1.4453\mathrm{i}$
U2	$-1.8940 - 8.9215\mathrm{i}$	$-1.9078 - 9.0347\mathrm{i}$	$-1.9169 - 9.07189\mathrm{i}$	$-1.9046 - 9.0579\mathrm{i}$	$-1.9192 - 9.0814\mathrm{i}$

Table 2: Effect of the boundary condition on the position of the most cut-on eigenvalues for the canonical case $M_x = M_\theta = 0.5$, $h = 0.5$, $\omega = 4$, $m = -1$, $Z_h = Z_1 = 1 - \mathrm{i}$. **U1**: 1st upstream mode, **U2**: 2nd upstream mode, **D1**: 1st downstream mode, **D2**: 2nd downstream mode.

C. Centrifugal effect on the eigenmodes at lower frequency

Because of the ω^{-1} factor contained in the centrifugal term in Eqs. (37) and (38), larger differences are expected between the old Myers boundary condition and the new Myers boundary condition in the low-frequency range. To illustrate this, the above test is considered with a frequency ten times lower ($\omega = 0.4$), all the other parameters being unchanged. The eigenvalues obtained with both boundary conditions are plotted in Fig. 1. They are compared to the eigenvalues of reference which have been computed for a realistic flow profile defined by $U_x(r) = U_\theta(r) = 0.5 \times L_{2500}(r)$, where L_{2500} represents a thin boundary layer ($\varepsilon = 4 \times 10^{-4}$).

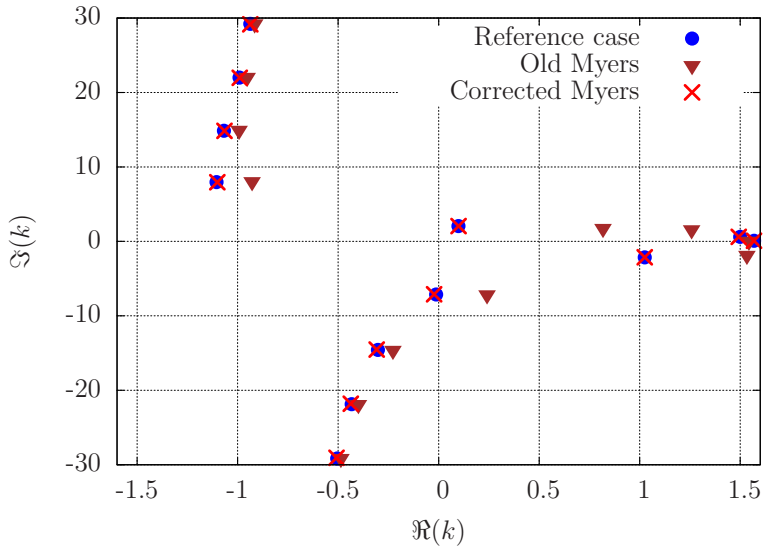

Figure 1: Eigenvalues position in the complex k-plane at low frequency ($\omega = 0.4$). The case is defined by $M_x = M_\theta = 0.5$, $h = 0.5$, $m = -1$, $Z_h = Z_1 = 1 - \mathrm{i}$.

As expected, the centrifugal effects in the boundary condition are much stronger than for the previous frequency of observation. Indeed, for this specific case, $Z_h^\ddagger = 1 + 0.13\mathrm{i}$ and $Z_1^\ddagger = 1 - 1.67\mathrm{i}$. The old Myers boundary condition inaccurately predicts the eigenvalues while the new boundary condition gives solutions much closer to the reference.

D. Illustration of the correct behavior for vanishing boundary layers

In this section, the exact value of $Z^1_{\text{eff}} = \hat{p}^1_\infty / \hat{u}^1_\infty$, which would be obtained if there was no boundary layer is compared with the effective impedance arising from the different boundary conditions. The parameters used for the study are $h = 0.5$, $\omega = 5$, $m = 1$ and $M_x = M_\theta = 0.5$. Using an envelope similar to L_α, an exponential boundary layer is specified at the outer wall only. At the inner wall, the arbitrary boundary condition is defined so that $-\hat{p}(h)/\hat{u}(h) = -\hat{p}^h_\infty / \hat{u}^h_\infty = Z = 1 - \mathrm{i}$. Using this boundary condition and the governing equations (15) and (16) allows calculating the exact value of $\hat{p}^1_\infty$ and $\hat{v}^1_\infty$ at the outer wall, when

there is no boundary layer. If the boundary layer is present, the exact value of $Z^1_{BL} = \hat{p}_\alpha(1)/\hat{u}_\alpha(1)$ can be computed in the same way. Since then, the accuracy of the boundary conditions can be assessed by comparing the exact value $Z^1_{\text{eff}} = \hat{p}^1_\infty/\hat{u}^1_\infty$ with the ones which would be obtained by inserting Z^1_{BL} in the boundary conditions. The new boundary condition, the approximated boundary condition and the classical Myers boundary condition are written in terms of an effective impedance. They read

$$Z^{\star,1}_{\text{eff}} = -\frac{\omega}{\Lambda^1_\infty}\left(Z^1_{BL} + \frac{\mathrm{i}}{\omega}\int_{R_m}^1 \rho_0 \frac{\mathrm{d}}{\mathrm{d}r}\left(U^2_\theta\right)\mathrm{d}r\right), \tag{47}$$

$$Z^{\ddagger,1}_{\text{eff}} = -\frac{\omega}{\Lambda^1_\infty}\left(Z^1_{BL} - \frac{\mathrm{i}}{\omega}\rho_0^{\text{nbl}}(1)M^2_{\theta,1}\right), \tag{48}$$

$$Z^{M,1}_{\text{eff}} = -\frac{\omega Z^1_{BL}}{\Lambda^1_\infty}, \tag{49}$$

respectively. For these three boundary conditions, the equivalent impedance is compared with Z^1_{eff}. In Fig 2, the evolution of the errors $|Z^{\star,1}_{\text{eff}}/Z^1_{\text{eff}} - 1|$, $|Z^{\ddagger,1}_{\text{eff}}/Z^1_{\text{eff}} - 1|$ and $|Z^{M,1}_{\text{eff}}/Z^1_{\text{eff}} - 1|$ as a function of the boundary layer thickness are shown for four values of k: 1, -1, $1+\mathrm{i}$ and $-1-\mathrm{i}$.

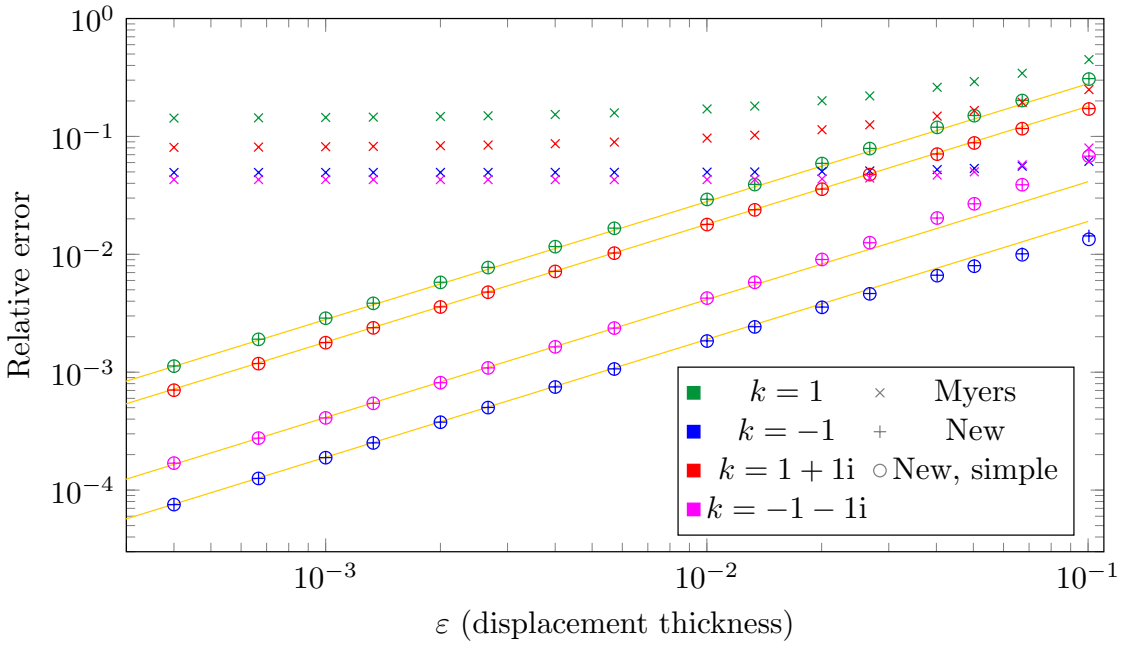

Figure 2: Plot of the relative error $|Z^{\star,1}_{\text{eff}}/Z^1_{\text{eff}} - 1|$ (plusses), $|Z^{\ddagger,1}_{\text{eff}}/Z^1_{\text{eff}} - 1|$ (circles) and $|Z^{M,1}_{\text{eff}}/Z^1_{\text{eff}} - 1|$ (crosses) at the outer wall. $h = 0.5$, $\omega = 5$, $m = 1$ and $M_x = M_\theta = 0.5$.

Since the corrected Myers boundary condition has been developed to leading order in δ, it is expected that the error decreases linearly with the boundary layer thickness. The linear relationship between the error and the boundary layer thickness is drawn in yellow. The corrected Myers boundary condition as well as its approximation match pretty well the expected behavior while the classical Myers condition is clearly wrong.

Applying the same procedure at the inner wall leads to the same conclusions. Comparisons have not been shown here for the sake of conciseness.

E. A realistic turbofan engine configuration: the SDT test case

Finally, the corrected Myers boundary condition is tested on a realistic fan configuration. The mean flow has been extracted from a RANS simulation performed on the NASA SDT test case[19,20] so that the flow is representative of a bypass interstage. After interpolating the mean flow on a set of rational functions, a boundary layer can be added by multiplying the mean flow by the exponential envelope defined in Eq. (43).

We have chosen $\alpha = 200$ since it corresponds to a displacement thickness of $\varepsilon = 0.01$, which is representative of a boundary layer thickness in the interstage. The mean flow profiles with or without the boundary layer are shown in Fig. 3(a) and 3(b).

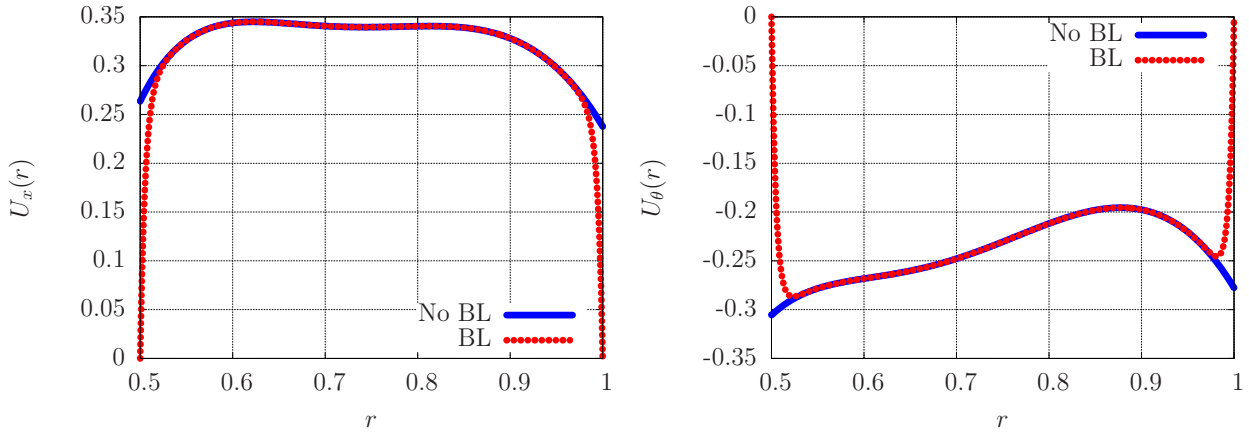

(a) Axial profile

(b) Azimuthal profile

Figure 3: Interpolated profiles from the SDT test case, with or without a boundary layer.

The SDT test case has been built such that $h = 0.5$. The frequency of the study is chosen so that it fit with the maximum of the rotor stator interaction broadband noise spectra in approach condition. $f^*_{maxdB} = 3000$ Hz has been taken from Masson *et al.*,[21] which corresponds to $\omega = 15$. Even if there is no acoustic treatment in the NASA SDT, the wall are assumed to be lined with typical acoustic treatments. The impedance is set to $Z_h = Z_1 = 2.55 + 1.5\mathrm{i}$. The imaginary part is a bit above zero which means a resonance at a slightly higher frequency. The effect of the boundary condition on the eigenvalues and the eigenfunctions will be assessed for $m = 1$ and $m = 15$. Since the azimuthal flow is negative, these values correspond to contra-rotating modes according to the conventions of the paper.

1. *Position of the eigenvalues*

The azimuthal mode $m = 1$ is considered first. The eigenvalues solutions of Eq. (39) are plotted in Fig. 4 for three boundary conditions. The old Myers boundary condition (Eq. (17), violet triangles) and the new corrected Myers boundary condition (Eq. (38), red crosses) are compared with the reference (Eq. (45), blue circles) which is obtained by considering the boundary layer near the walls. For these three cases, the same boundary condition is applied both at the inner wall and at the outer wall.

Since the frequency is quite high, results obtained from the old Myers boundary condition and from the corrected Myers boundary condition are really similar, the eigenvalues being almost indistinguishable. The "most" cut-on modes, which are the most relevant when studying in-duct transmission, are pretty well predicted, especially in the downstream direction, while the accuracy decreases as the modes move away from the real axis.

Second, the same methodology is applied for the azimuthal mode order $m = 15$. The results are presented in Fig. 5. Once again, the old Myers boundary condition gives very similar results to the corrected one. However, significant error is observed with respect to the case of reference, even for the eigenvalues located close to the real axis. This is expected to alter the prediction when acoustic transmission is considered. To improve the accuracy of the corrected Myers boundary condition with swirl, it is possible to extend the method presented in section II to the first order in δ, as done by Brambley.[6] This extension is developed in Mathews *et al.*[16] and shows a noticeable improvement in terms of prediction.

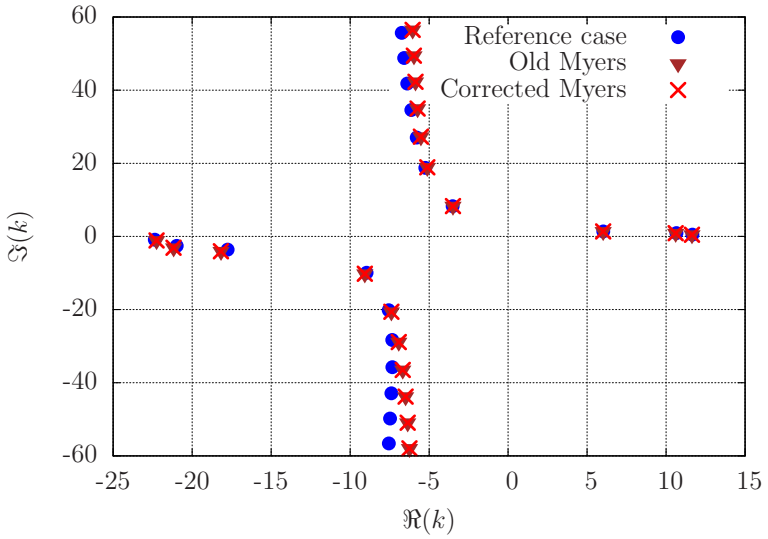

Figure 4: Eigenvalues position in the complex k-plane for a realistic test case based on the SDT mean flow. The case is defined by $\omega = 15$, $h = 0.5$, $m = 1$, $Z_h = Z_1 = 2.55 + 1.5\mathrm{i}$.

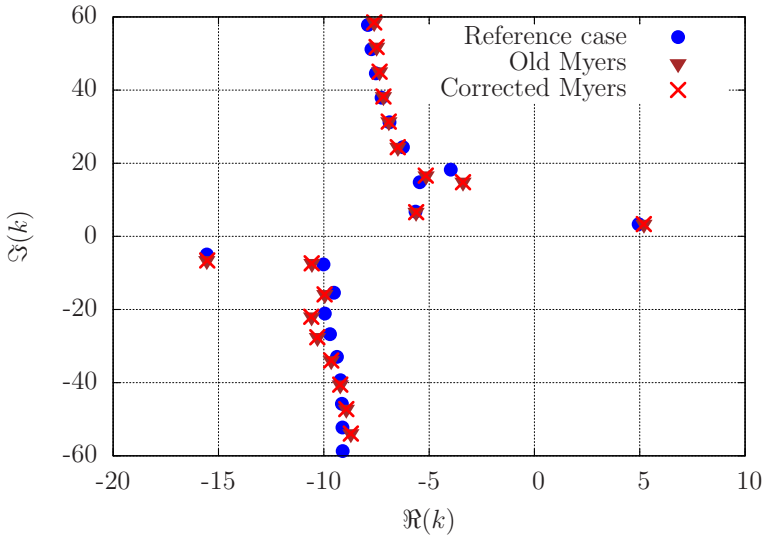

Figure 5: Eigenvalues position in the complex k-plane for a realistic test case based on the SDT mean flow. The case is defined by $\omega = 15$, $h = 0.5$, $m = 15$, $Z_h = Z_1 = 2.55 + 1.5\mathrm{i}$.

V. Acoustic transmission in a rigid annular duct with a finite lined section

A. The mode-matching methods

Sound transmission through a finite lined section inside a rigid duct and the associated transmission loss is a good way to characterize the efficiency of a locally reacting liner. The presence of impedance discontinuities in the duct generates a modal scattering and requires using a mode matching method. The different modal contents in both the rigid and the lined sections are matched at the interface by means of conservation relationships. The "classical" formalism relies on the conservation of the fluctuating pressure and axial velocity at the interface, which is equivalent to the conservation of the mass flow and the total enthalpy in the case of an axial mean flow.[22] In this paper, a formulation based on the conservation of the mass flow and the total enthalpy is also used. It is shown however that this does not reduce to the conservation of the pressure and the axial velocity in presence of a swirling flow. A projection basis based on Chebyshev

polynomials is proposed to improve the accuracy of the method. Guan *et al.*[10] also studied the influence of the swirl on the acoustic transmission. They used an extended mode-matching method based on a variational formulation of the Navier-Stokes equations and developed by Gabard & Astley.[23]

B. Formalism

The acoustic transmission through a lined section at a given frequency ω is studied in this section. An infinite rigid annular duct containing a finite lined section is considered. A mean flow with the same properties as in section I is considered. The axial and the azimuthal profiles of the mean flow remain unchanged along the duct axis so that the matching across the interfaces applies on the perturbations only. The surface impedances of the liner are referred to as Z_h and Z_1 at hub and tip respectively. They may vary with the frequency. A sketch of the physical statement is represented in Fig. 6.

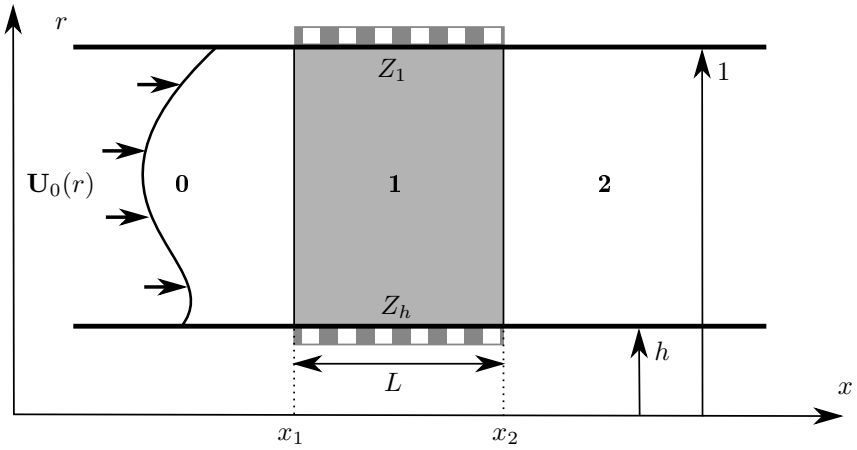

Figure 6: Lined section in an infinite rigid annular duct.

In Fig. 6 the mean flow propagates from left to right. The duct is split into three zones. Zone 0 spreads from the upstream infinite to the beginning of the lined section; the lined segment of length L is referred to as zone 1; while zone 2 extends from the end of the lined section to the downstream infinite. Attention is paid to the transmission of acoustic waves initially propagating from left to right.

In the following, a more general formalism is considered to deal with an impedance discontinuity in the axial direction. The axial coordinate of the interface located between zone $l-1$ and zone l is noted x_l. The surface impedances are assumed constant in the azimuthal direction and do not vary axially inside a given segment. Since the physical statement does not present any change along the azimuthal direction, no scattering occurs in azimuthal mode order and only radial scattering will be considered for a given azimuthal mode of the acoustic variables. Therefore, the problem can be treated in the plane (r, x) and the index m of the considered circumferential mode may be kept implicitly in order to clarify the notations. For that given mode, eigenvalues and eigenfunctions are supposed to be known initially in all the considered zones so that the fluctuating pressure, the tangential and the axial velocity in zone l can be expanded as

$$p_l(x,r) = \sum_{\mu=1}^{\mu_{\max}} A^+_{l,\mu}\Psi^+_{l,\mu}(r)e^{\mathrm{i}k^+_{l,\mu}(x-x_{l+1})} + A^-_{l,\mu}\Psi^-_{l,\mu}(r)e^{\mathrm{i}k^-_{l,\mu}(x-x_l)} \tag{50}$$

$$v_l(x,r) = \sum_{\mu=1}^{\mu_{\max}} A^+_{l,\mu}V^+_{l,\mu}(r)e^{\mathrm{i}k^+_{l,\mu}(x-x_{l+1})} + A^-_{l,\mu}V^-_{l,\mu}(r)e^{\mathrm{i}k^-_{l,\mu}(x-x_l)} \tag{51}$$

$$w_l(x,r) = \sum_{\mu=1}^{\mu_{\max}} A^+_{l,\mu}W^+_{l,\mu}(r)e^{\mathrm{i}k^+_{l,\mu}(x-x_{l+1})} + A^-_{l,\mu}W^-_{l,\mu}(r)e^{\mathrm{i}k^-_{l,\mu}(x-x_l)} \tag{52}$$

where $A_{l,\mu}$ and $k_{l,\mu}$ stand for the modal amplitude and the axial wave number of the μ-th radial mode in zone l. The subscript "+" stands for the upstream propagating modes while the subscript "−" stands for the downstream propagating modes. The origins to define $A^\pm_{l,\mu}$ and the associated phase shifts are set so that only decaying waves propagate inside the different zones and only decaying exponential terms appear.

Namely, the origin is set on the right extremity of the zone for the upstream-going acoustic waves while it is set on the left extremity for the downstream-going ones. Fig. 7 summarizes the present conventions. [b]

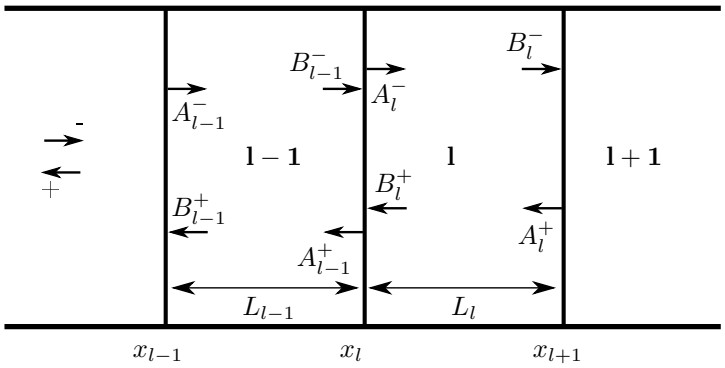

Figure 7: Sketch of a general mode matching formulation at an interface between two segments with different modal contents.

In Eqs. (50), (51) and (52), $\Psi_{l,\mu}$, $V_{l,\mu}$ and $W_{l,\mu}$ are the eigenfunctions of the μ-th mode for the pressure, the azimuthal and the axial fluctuating velocity respectively. They can be determined previously by solving an eigenvalue problem for example. Taking the same modal amplitudes $A_{l,\mu}$ for the pressure and the axial velocity imposes the following relationships:[24]

$$V_{l,\mu}(r) = -\frac{1}{\rho_0(r)D_\mu(r)}\left[\frac{\mathrm{d}(rU_\theta(r))}{r\mathrm{d}r}\frac{\mathrm{d}\Psi_{l,\mu}(r)}{\mathrm{d}r} + \left(\frac{mD_\mu(r)}{r\Lambda_\mu(r)} + B_\mu(r)\frac{\mathrm{d}(rU_\theta(r))}{r\mathrm{d}r}\right)\Psi_{l,\mu}(r)\right], \tag{53}$$

$$W_{l,\mu}(r) = -\frac{1}{\rho_0(r)D_\mu(r)}\left[\frac{\mathrm{d}U_{xd}(r)}{\mathrm{d}r}\frac{\mathrm{d}\Psi_{l,\mu}(r)}{\mathrm{d}r} + \left(\frac{k_{l,\mu}D_\mu(r)}{\Lambda_\mu(r)} + B_\mu(r)\frac{\mathrm{d}U_{xd}(r)}{\mathrm{d}r}\right)\Psi_{l,\mu}(r)\right]. \tag{54}$$

where D_μ, Λ_μ and B_μ are the flow functions introduced in Posson & Peake.[11] They are recalled in appendix A.

C. Matching conditions

As usually done in the uniform case, the matching conditions rely on the conservation of mass and total enthalpy through the interface between the two considered segments. An infinite fluid channel located between the radii r and $r+\mathrm{d}r$ and bounded by the azimuthal coordinates $[\theta, \theta+\mathrm{d}\theta]$ is considered such that the surface of the interface located at the axial position x_l is defined by $\mathrm{d}S = r\mathrm{d}r\mathrm{d}\theta$. The mass conservation at the interface reads:

$$\mathrm{d}S\rho_{to,l-1}(x_l,r)\mathbf{U}_{to,l-1}(x_l,r)\cdot\mathbf{n} = \mathrm{d}S\rho_{to,l}(x_l,r)\mathbf{U}_{to,l}(x_l,r)\cdot\mathbf{n}, \tag{55}$$

where $\mathbf{n}$ is normal to the interface. The latter reduces to $\mathbf{e}_x$ in the present case. The conservation of the total enthalpy h_{tot} through the interface reads:

$$h_{tot,l-1}(x_l,r) = h_{tot,l}(x_l,r), \tag{56}$$

with

$$h_{tot,l}(x,r) = h_l(x,r) + \frac{\|\mathbf{U}_{to,l}(x,r)\|^2}{2}$$

where $h_l(x_l,r) = c_pT_{l,to}(x_l,r)$ is the enthalpy of the flow in the segment l, c_p and $T_{l,to}$ being the thermal capacity and the temperature respectively. Eqs. (55) and (56) are expanded and linearized by introducing small perturbations around a stationary mean flow. Assuming isentropic fluctuations, the matching conditions reduce to:

$$\left[\frac{U_x(r)}{c_0^2(r)}p(x_l,r) + \rho_0(r)w(x_l,r)\right]_{l-1}^{l} = 0, \tag{57}$$

[b] Concerning the specific case of downstream-going waves in zone 0, the origin is taken at $x_0 = x_1 - L_1$. Similarly, the phase origin for the upstream-going waves in zone 2 is taken at the axial location $x_3 = x_2 + L_3$, where L_1 and L_3 are arbitrary lengths.

$$\left[\frac{p(x_l,r)}{\rho_0(r)} + U_\theta(r)v(x_l,r) + U_x(r)w(x_l,r)\right]_{l-1}^{l} = 0\,. \tag{58}$$

Using the previous modal decomposition given by Eqs. (50) - (52), Eqs. (57) and (58) can be projected on a family of radial functions $(\Phi_\nu)_{\nu=0,\dots,\mu_{\max}-1}$ to obtain as many equations as unknowns $A^{\pm}_{l,\mu}$. It reads:

$$\left\langle \frac{U_x}{c_0^2}p_{l-1}(x_l) + \rho_0 w_{l-1}(x_l), \Phi^1_\nu \right\rangle = \left\langle \frac{U_x}{c_0^2}p_l(x_l) + \rho_0 w_l(x_l), \Phi^1_\nu \right\rangle, \quad \nu = 0,\dots,\mu_{\max}-1, \tag{59}$$

and

$$\left\langle \frac{p_{l-1}(x_l)}{\rho_0} + U_\theta v_{l-1}(x_l) + U_x w_{l-1}(x_l), \Phi^2_\nu \right\rangle = \left\langle \frac{p_l(x_l)}{\rho_0} + U_\theta v_l(x_l) + U_x w_l(x_l), \Phi^2_\nu \right\rangle, \quad \nu = 0,\dots,\mu_{\max}-1, \tag{60}$$

where $\langle\cdot\rangle$ is an inner product for which the set of $(\Phi_\nu)_{\nu=0,\dots,\mu_{\max}-1}$ forms an independent set.

D. Choice of the projection basis

Since the linear system of section III is solved using a pseudo-spectral method, each eigenfunction is a linear combination of the N first Chebyshev polynomials. For example, the μ-th acoustic pressure eigenfunction is defined by:

$$\Psi_\mu(r) = \widetilde{\Psi}_\mu(\xi) = \sum_{k=0}^{N-1} a_{k,\mu}T_k(\xi). \tag{61}$$

where N is the number of collocation points used for the pseudo-spectral method, T_k is the Chebyshev polynomial defined by:

$$T_k(\xi) = \cos\left(k\cos^{-1}(\xi)\right), \tag{62}$$

with $\xi \in [-1,1]$ is defined by:

$$\xi = \left(\frac{2}{h-1}\right)\left[r - \left(\frac{h+1}{2}\right)\right]. \tag{63}$$

The choice of the projection functions Φ^1_ν and Φ^2_ν as well as the inner product is quite important. In most of the in-duct transmission problems, the inner product defined by

$$\langle f,g\rangle_c = \int_h^1 r f(r)g(r)\mathrm{d}r \tag{64}$$

is used, since it is orthogonal for the set of Bessel's functions.[25] When the swirl of the mean flow is non-zero, the eigenfunctions are no longer orthogonal.[26] In particular, the property $\langle\Psi_\mu,\Psi_\nu\rangle_c = \delta_{\mu,\nu}$ that is satisfied by the Bessel eigenfunctions in the case of a uniform axial flow no longer holds.

Another inner product can be defined, (see Boyd,[27] section A.2):

$$\langle f,g\rangle = \frac{2}{\pi}\int_{-1}^{1}\frac{f(\xi)g(\xi)}{\sqrt{1-\xi^2}}\mathrm{d}\xi. \tag{65}$$

This inner product is particularly well suited to the Chebyshev polynomials. In particular,

$$\langle T_m,T_n\rangle = \begin{cases} 0 & \text{for } m \neq n \\ 1/2 & \text{for } m = n = 0\,. \\ 1 & \text{for } m = n \neq 0 \end{cases} \tag{66}$$

Therefore, $(T_k)_{k=0,\dots,N-1}$ forms an orthogonal basis for the set of the continuous eigenfunctions defined in $[-1,1]$. In particular,

$$\langle\widetilde{\Psi}_\mu,T_0\rangle = \frac{a_{0,\mu}}{2}, \qquad \langle\widetilde{\Psi}_\mu,T_\nu\rangle = a_{\nu,\mu}, \qquad \nu = 1,\dots,\mu_{\max}-1. \tag{67}$$

Assuming the $a_{k,\mu}$ coefficients are known, the use of this inner product coupled with the set of projection functions $\Phi^1_\nu(r) = \Phi^2_\nu(r) = T_{\nu-1}(\xi)$ would allow avoiding the computation of the integrals usually required for the projections. Instead, only one inversion of a N^2 matrix is necessary to determine the set of $(a_{k,\mu})_{k=0,\dots,N-1}$, which leads to more accurate results than a numerical integration.

E. Application to the matching of the conservative variables

Let $\Theta_{l,\mu}$ and $\Upsilon_{l,\mu}$ two radial functions such that:

$$\Theta_{l,\mu}(r) = \frac{U_x(r)}{c_0^2(r)}\Psi_{l,\mu}(r) + \rho_0(r)W_{l,\mu}(r), \tag{68}$$

and

$$\Upsilon_{l,\mu}(r) = \frac{\Psi_{l,\mu}(r)}{\rho_0(r)} + U_\theta(r)V_{l,\mu}(r) + U_x(r)W_{l,\mu}(r). \tag{69}$$

Replacing $p_l(x_l)$, $v_l(x_l)$ and $w_l(x_l)$ in Eqs. (59) and (60) by their modal expansions given in Eqs. (50) and (52) gives the set of $2\mu_{\max}$ equations:

$$\sum_{\mu=1}^{\mu_{\max}} A_{l,\mu}^+ a_{l,\nu\mu}^+ e^{\mathrm{i}k_{l,\mu}^+(x_l-x_{l+1})} + A_{l,\mu}^- a_{l,\nu\mu}^- = \sum_{\mu=1}^{\mu_{\max}} A_{l-1,\mu}^+ a_{l-1,\nu\mu}^+ + A_{l-1,\mu}^- a_{l-1,\nu\mu}^- e^{\mathrm{i}k_{l-1,\mu}^-(x_l-x_{l-1})},$$
$$\sum_{\mu=1}^{\mu_{\max}} A_{l,\mu}^+ b_{l,\nu\mu}^+ e^{\mathrm{i}k_{l,\mu}^+(x_l-x_{l+1})} + A_{l,\mu}^- b_{l,\nu\mu}^- = \sum_{\mu=1}^{\mu_{\max}} A_{l-1,\mu}^+ b_{l-1,\nu\mu}^+ + A_{l-1,\mu}^- b_{l-1,\nu\mu}^- e^{\mathrm{i}k_{l-1,\mu}^-(x_l-x_{l-1})},$$

$$\nu = 1, \ldots, \mu_{\max},$$

where

$$a_{l,\nu\mu}^\pm = \langle \Theta_{l,\mu}^\pm, \Phi_\nu^1 \rangle, \qquad b_{l,\nu\mu}^\pm = \langle \Upsilon_{l,\mu}^\pm, \Phi_\nu^2 \rangle.$$

The previous system of equations may be rewritten in the matrix form:

$$\mathbf{a}_l^+\mathbf{B}_l^+ + \mathbf{a}_l^-\mathbf{A}_l^- = \mathbf{a}_{l-1}^+\mathbf{A}_{l-1}^+ + \mathbf{a}_{l-1}^-\mathbf{B}_{l-1}^- \tag{70}$$
$$\mathbf{b}_l^+\mathbf{B}_l^+ + \mathbf{b}_l^-\mathbf{A}_l^- = \mathbf{b}_{l-1}^+\mathbf{A}_{l-1}^+ + \mathbf{b}_{l-1}^-\mathbf{B}_{l-1}^- \tag{71}$$

where $\mathbf{A}_l$ and $\mathbf{B}_l$ are the vectors defined by:

$$(\mathbf{A}_l^\pm)_\mu = A_{l,\mu}^\pm, \qquad (\mathbf{B}_l^-)_\mu = A_{l,\mu}^- e^{\mathrm{i}k_{l,\mu}^-(x_{l+1}-x_l)}, \qquad (\mathbf{B}_l^+)_\mu = A_{l,\mu}^+ e^{\mathrm{i}k_{l,\mu}^+(x_l-x_{l+1})},$$

and where $\mathbf{a}_l$ and $\mathbf{b}_l$ are the matrices defined by:

$$(\mathbf{a}_l^\pm)_{\nu,\mu} = a_{l,\nu\mu}^\pm, \qquad (\mathbf{a}_l^\pm)_{\nu,\mu} = a_{l,\nu\mu}^\pm.$$

In most of the transmission problems, it is convenient to express $\mathbf{A}_{l-1}^-$ and $\mathbf{A}_l^+$ as a function of the incident field $\mathbf{B}_{l-1}^-$ and $\mathbf{B}_l^+$ on the interface x_l. Therefore, Eqs. (70) and (71) are restated so that the unknowns $\mathbf{A}_{l-1}^-$ and $\mathbf{A}_l^+$ remain on the left-hand side of the equations. It reads:

$$\mathbf{a}_l^-\mathbf{A}_l^- - \mathbf{a}_{l-1}^+\mathbf{A}_{l-1}^+ = -\mathbf{a}_l^+\mathbf{B}_l^+ + \mathbf{a}_{l-1}^-\mathbf{B}_{l-1}^- \tag{72}$$
$$\mathbf{b}_l^-\mathbf{A}_l^- - \mathbf{b}_{l-1}^+\mathbf{A}_{l-1}^+ = -\mathbf{b}_l^+\mathbf{B}_l^+ + \mathbf{b}_{l-1}^-\mathbf{B}_{l-1}^-. \tag{73}$$

The latter relationship can be rewritten in a more concise way:

$$\mathbf{T}_{l,1}\begin{pmatrix} \mathbf{A}_l^- \\ \mathbf{A}_{l-1}^+ \end{pmatrix} = \mathbf{T}_{l,2}\begin{pmatrix} \mathbf{B}_l^+ \\ \mathbf{B}_{l-1}^- \end{pmatrix},$$

with

$$\mathbf{T}_{l,1} = \begin{pmatrix} \mathbf{a}_l^- & -\mathbf{a}_{l-1}^+ \\ \mathbf{b}_l^- & -\mathbf{b}_{l-1}^+ \end{pmatrix}, \quad \text{and} \quad \mathbf{T}_{l,2} = \begin{pmatrix} -\mathbf{a}_l^+ & \mathbf{a}_{l-1}^- \\ -\mathbf{b}_l^+ & \mathbf{b}_{l-1}^- \end{pmatrix}.$$

Finally, the scattering matrix $\mathbf{S}_l$ is introduced so that

$$\begin{pmatrix} \mathbf{A}_l^- \\ \mathbf{A}_{l-1}^+ \end{pmatrix} = \mathbf{S}_l\begin{pmatrix} \mathbf{A}_l^+ \\ \mathbf{A}_{l-1}^- \end{pmatrix}. \tag{74}$$

Consequently,

$$\mathbf{S}_l = \mathbf{T}_{l,1}^{-1}\mathbf{T}_{l,2}\mathbf{X}_l. \tag{75}$$

where $\mathbf{X}_l$ is the diagonal matrix of the phase shift defined by:

$$\mathbf{X}_l = \begin{pmatrix} \mathbf{X}_l^+ & \mathbf{0} \\ \mathbf{0} & \mathbf{X}_{l-1}^- \end{pmatrix},$$

where

$$(\mathbf{X}_l^+)_{\nu,\mu} = \delta_{\mu,\nu} e^{\mathrm{i}k_{l,\mu}^+(x_l - x_{l+1})}, \quad (\mathbf{X}_{l-1}^-)_{\nu,\mu} = \delta_{\mu,\nu} e^{\mathrm{i}k_{l-1,\mu}^-(x_l - x_{l-1})}.$$

Therefore, according to the previous developments, the matching condition at both interfaces x_1 and x_2 in Fig. 6 reads:

$$\begin{pmatrix} \mathbf{A}_1^- \\ \mathbf{A}_0^+ \end{pmatrix} = \mathbf{S}_1 \begin{pmatrix} \mathbf{A}_1^+ \\ \mathbf{A}_0^- \end{pmatrix}, \quad \begin{pmatrix} \mathbf{A}_2^- \\ \mathbf{A}_1^+ \end{pmatrix} = \mathbf{S}_2 \begin{pmatrix} \mathbf{A}_2^+ \\ \mathbf{A}_1^- \end{pmatrix}.$$

Assuming the matrices S_1 and S_2 are known, the overall scattering matrix $\mathbf{S}$, which verifies

$$\begin{pmatrix} \mathbf{A}_2^- \\ \mathbf{A}_0^+ \end{pmatrix} = \mathbf{S} \begin{pmatrix} \mathbf{A}_2^+ \\ \mathbf{A}_0^- \end{pmatrix} \tag{76}$$

can be determined thanks to the relationship:

$$\mathbf{S} = \mathbf{S}_1 \otimes \mathbf{S}_2, \tag{77}$$

where $\otimes$ stands for the Redheffer product[28,29] defined by:

$$\mathbf{A} \otimes \mathbf{B} = \begin{pmatrix} \mathbf{B}_{11}(\mathbf{I} - \mathbf{A}_{12}\mathbf{B}_{21})^{-1}\mathbf{A}_{11} & \mathbf{B}_{12} + \mathbf{B}_{11}\mathbf{A}_{12}(\mathbf{I} - \mathbf{B}_{21}\mathbf{A}_{12})^{-1}\mathbf{B}_{22} \\ \mathbf{A}_{21} + \mathbf{A}_{22}\mathbf{B}_{21}(\mathbf{I} - \mathbf{A}_{12}\mathbf{B}_{21})^{-1}\mathbf{A}_{11} & \mathbf{A}_{22}(\mathbf{I} - \mathbf{B}_{21}\mathbf{A}_{12})^{-1}\mathbf{B}_{22} \end{pmatrix} \tag{78}$$

where $\mathbf{A}_{ij}$ and $\mathbf{B}_{ij}$ are squared matrices in the present case. The method of Redheffer product has been used previously in mode-matching problems (see Oppeneer[30] for example). This method offers the advantage to be direct in comparison with iterative methods. The result is then obtained in a faster way. Besides the choice of the phase origins allows avoiding spurious instabilities since only decaying exponential are induced by this choice.

F. Transmission loss

The transmission loss is defined as the acoustic power absorbed by the lined section. By definition, it reads:

$$\mathbf{TL}_{\mathrm{dB}} = \mathrm{P}_i - \mathrm{P}_t, \tag{79}$$

where P_i and P_t are the incident and the transmitted power respectively. Since the mean flow is not necessarily irrotational, the Myers[31] generalized formalism will be used to compute the acoustic power, as done in Posson & Peake.[24] From the Myers formalism, an acoustic power flow across the volume surface S of outer normal $\mathbf{n}$ can be defined by:

$$\mathrm{P}(x) = \mathrm{Re}\left(\iint_{S(x)} \mathbf{I}(r,x) \cdot \mathbf{n} \mathrm{d}S \right), \tag{80}$$

where Re refers to the real part and $\mathbf{I}$ is the acoustic intensity defined by

$$\mathbf{I}(r,x) = \left(\frac{p(r,x)}{\rho_0(r)} + \mathbf{u}(r,x) \cdot \mathbf{U_0}(r) \right) \left(\overline{\rho_0(r)\mathbf{u}(r,x) + \rho(r,x)\mathbf{U_0}(r)} \right), \tag{81}$$

where the overline stands for the complex conjugate.

When studying in-duct acoustic power, it can be convenient to consider a surface normal to the duct axis. In that case, $\mathbf{n} = \mathbf{n}^{\pm} = \mp \mathbf{e}_x$. Then the acoustic intensity writes:

$$\mathbf{I}(r,x) \cdot \mathbf{n}^{\pm} = \mp \left(\frac{p(r,x)}{\rho_0(r)} + v(r,x)U_\theta(r) + w(r,x)U_x(r) \right) \left(\overline{\rho_0(r)w(r,x) + \frac{Ux(r)}{c_0^2(r)} p(r,x)} \right),$$

and the integration over $S(x)$ reduces directly to an integration over r and θ. Since the integrand does not depend on the θ parameter, the acoustic power reduces to an integral over the r coordinate only:

$$\mathbf{P}^{\pm}(x) = \mathrm{Re}\left\{2\pi \int_h^1 \left[\mathbf{I}(r,x)\cdot\mathbf{n}^{\pm}\right] \mathrm{d}r\right\}.$$

The two terms contained in the integrand can be identified as the fluctuations of mass and total enthalpy, as defined in Eqs. (57) and (58) for example. Since then, considering a single acoustic liner in section $l = 1$, inside an infinite duct, as in Figure 6, the transmitted power reads:

$$\mathrm{P}_t(x) = \mathrm{P}_2^-(x) = \mathrm{Re}\left\{2\pi \int_h^1 \left(\sum_{\mu=1}^{\mu_{\max}} A_{2,\mu}^- \Upsilon_{2,\mu}^-(r) e^{\mathrm{i}k_{2,\mu}^-(x-x_2)}\right)\left(\overline{\sum_{\nu=0}^{\mu_{\max}} A_{2,\nu}^- \Theta_{2,\nu}^-(r) e^{\mathrm{i}k_{2,\nu}^-(x-x_2)}}\right)\mathrm{d}r\right\}, \quad x > x_2, \tag{82}$$

and similarly the reflected power:

$$\mathrm{P}_r(x) = \mathrm{P}_0^+(x) = \mathrm{Re}\left\{2\pi \int_h^1 \left(\sum_{\mu=1}^{\mu_{\max}} A_{0,\mu}^+ \Upsilon_{0,\mu}^+(r) e^{\mathrm{i}k_{0,\mu}^+(x-x_1)}\right)\left(\overline{\sum_{\nu=0}^{\mu_{\max}} A_{0,\nu}^+ \Theta_{0,\nu}^+(r) e^{\mathrm{i}k_{0,\nu}^+(x-x_1)}}\right)\mathrm{d}r\right\}, \quad x < x_1. \tag{83}$$

By supposing that the cross-term are negligible, the transmitted and reflected acoustic powers are directly obtained as the sum of the transmitted and reflected acoustic power related to the mode μ and are independent from x:

$$\mathrm{P}_t = \sum_{\mu=1}^{\mu_{\max}} \mathrm{P}_{t,\mu}\,, \quad \mathrm{P}_r = \sum_{\mu=1}^{\mu_{\max}} \mathrm{P}_{r,\mu}\,,$$

with

$$\mathrm{P}_{t,\mu} = 2\pi |A_{2,\mu}^-|^2\, \mathrm{Re}\left\{\int_h^1 \Upsilon_{2,\mu}^-(r)\overline{\Theta_{2,\mu}^-(r)}\mathrm{d}r\right\}, \quad \mathrm{P}_{r,\mu} = 2\pi |A_{0,\mu}^+|^2\, \mathrm{Re}\left\{\int_h^1 \Upsilon_{0,\mu}^+(r)\overline{\Theta_{0,\mu}^+(r)}\mathrm{d}r\right\}.$$

G. Modal intensity

Finally, it is convenient, for results analysis, to define the associated mean modal transmitted and reflected intensities through the duct section, related to the mode μ, $I_{t,\mu}$ and $I_{r,\mu}$, by

$$I_{.,\mu}^{\pm} = \frac{\mathbf{P}_{.,\mu}}{\pi(1-h^2)}, \quad . = t, r. \tag{84}$$

Mean intensities are presented in decibels, I_{dB}, with respect to the intensity of reference I_{ref}

$$I_{\mathrm{dB}} = 10\log_{10}\left(\frac{I}{I_{\mathrm{ref}}}\right), \tag{85}$$

where I_{ref} has been chosen to be consistent with (B.5) in Lidoine[25] in the case of a axial and uniform flow

$$I_{\mathrm{ref}} = (1 + U_x(1))p_{\mathrm{ref}}^2, \tag{86}$$

where $p_{\mathrm{ref}}^* = 2 \times 10^{-5}$ and $p_{\mathrm{ref}}^* = p_{\mathrm{ref}}\rho_0^*(R_t^*)c_0^{2*}(R_t^*)$.

VI. Results

The transmission losses are computed as follows. For a given couple (ω, m) and a given mean flow, only downstream cut-on radial modes in zone 0 are considered as incident modes. No sound is assumed to come from the right side of the domain, namely $A_{2,\mu}^+ = 0, \mu = 1, \ldots, \mu_{\max}$. From Eq. (84), the modal amplitudes of the incident cut-on modes can be expressed as a function of the incident modal intensity $I_{0,\mu}^-$:

$$A_{0,\mu}^- = \sqrt{\frac{I_{0,\mu}^-(1-h^2)}{2}\,\mathrm{Re}\left\{\left(\int_h^1 \Upsilon_{0,\mu}^-(r)\overline{\Theta_{0,\mu}^-(r)}\mathrm{d}r\right)^{-1}\right\}}. \tag{87}$$

In the present study, 100dB have been applied on each incident mode independently. The mode matching method is applied to determine the downstream acoustic intensity transmitted in zone 2 and the corresponding acoustic power on each radial modes. The first five cut-off modes have also been considered for the radial scattering. The projection method has first been validated by setting $Z_1 = Z_h = +\infty$, which corresponds to the case of a rigid central section. It has been verified for several couples (ω, m) that no radial scattering happens. A validation against available FEM tool in the case of no swirl is on-going.

To assess the effect of the swirl on the transmitted acoustic power, the same case as in section IV.E is considered. The mean flow has no boundary layer and the new Myers boundary condition is applied at the walls of the lined section. For the frequency $\omega = 15$ and the impedances $Z_h = Z_1 = 2.55 + 1.5\text{i}$, the opposite azimuthal mode orders $m = 1$ and $m = -1$ are considered. The non-dimensional length of the lined section is $L = 0.36$. The transmission losses obtained with the swirling and sheared mean flow presented in Fig 3(a) and 3(b) are compared with the ones obtained with the sheared flow only, the swirl being set to zero. In this last case, results are even with respect to m. For these three cases, 3 radial modes are cut-on in the rigid duct sections. The transmission losses are presented in Tables 3 to 5. Each row of the tables corresponds to a cut-on incident mode radial order. The integer at the top of each column refers to a transmitted radial mode order. First, the transmission losses for the non-swirling flow are presented in Table 3.

	1	2	3
1	15.4	31.8	29.5
2	44.0	26.8	55.7
3	63.4	86.5	43.7

Table 3: Transmission losses matrix for the no-swirl case. The parameters are $\omega = 15$, $Z_h = Z_1 = 2.55+1.5\text{i}$, $L = 0.36$, $m = 1$, the axial flow of Fig. 3(a) is used.

As expected, the lowest attenuation is located in the diagonal terms (at least 15dB lower than the off-diagonal terms). Second, the transmission losses for the swirling flow are presented in Table 4 for the contra-rotating mode $m = 1$ and in Table 5 for the co-rotating mode $m = -1$. As in the axial case, the lowest attenuation is located on the diagonal. The swirl has a noticeable effect on the liners absorption since the transmission losses may differ by up to 4dB in comparison with the axial flow case. Because of the swirl, the two opposite modes $m = 1$ and $m = -1$ now behave differently. For this specific case, accounting for the swirl mainly improves the absorption of the liner on the contra-rotating mode $m = 1$ while the sound absorption seems generally less efficient on the co-rotating mode $m = 1$.

	1	2	3
1	15.0	33.1	28.7
2	46.5	27.8	58.0
3	61.2	90.5	41.7

Table 4: Transmission losses matrix for the swirl case. The parameters are $\omega = 15$, $Z_h = Z_1 = 2.55 + 1.5\text{i}$, $L = 0.36$, $m = 1$, the axial flow of Fig. 3(a) and the azimuthal flow of Fig. 3(b) are used.

	1	2	3
1	15.3	30.2	30.2
2	39.6	24.1	52.9
3	63.2	90.1	43.1

Table 5: Transmission losses matrix for the swirl case. The parameters are $\omega = 15$, $Z_h = Z_1 = 2.55 + 1.5\text{i}$, $L = 0.36$, $m = -1$, the axial flow of Fig. 3(a) and the azimuthal flow of Fig. 3(b) are used.

Even if further investigations are required to draw general conclusions about the effect of swirl on the liner behavior, this example shows that the swirl has a significant effect on the liner absorption and then should be considered in attenuation modeling.

Conclusion and Future work

In this paper, a generalization of the Myers boundary condition has been developed in an annular duct with swirl, both for the inner wall and for the outer wall. It has been shown that the classical Myers boundary condition is not the correct limit when an infinitely thin boundary layer is considered at the walls in the presence of swirl. Indeed, centrifugal effects modify the boundary condition. The new boundary condition has the correct linear error behavior when the boundary layer thickness tends to zero. It is shown that using the classical Myers boundary condition can lead to significant error in the low-frequency range. The corrected boundary condition has been tested with a flow profile representative of a realistic turbofan bypass. If a typical boundary layer thickness is considered, results are still far from the reference. To improve the prediction, the boundary condition should be expanded to first order with respect to the boundary layer thickness. This method is presented in Mathews *et al.*[16]

Besides, a mode-matching method based on the conservation of the mass flow and the total enthalpy has been developed to evaluate the absorption of a duct-lined section in the presence of a possibly swirling and sheared mean flow. Unlike the axial-flow case, the latter does not reduce to the conservation of the acoustic pressure and the axial velocity when the swirl is non-zero. The mode-matching method relies on a new projection method based on the Chebyshev polynomials. First results have shown that the swirl may have a noticeable effect on the transmission losses and thus should be accounted for in transmission problems. In the future, the influence of the boundary condition on the liner absorption will be assessed after further validation of the present mode-matching method. The effect of the boundary layer shape on the boundary condition will also be assessed.

Acknowledgments

The authors would like to thank Pr. Michel Roger from École Centrale de Lyon, as well as Dr. Ed Brambley, Dr. Doran Khamis and Pr. Nigel Peake from the University of Cambridge for the interesting conversations about this topic and their precious advice. They are also grateful to Thomas Nodé-Langlois from Airbus for having provided the RANS data for the SDT test case. James Mathews was funded by ENOVAL, grant number MMZC/084 RG70800.

A. Swirl parameters

The following terms from Posson & Peake[11] are reminded in this appendix for clarity. They are introduced in section V.

$$\Lambda_\mu = k_\mu U_x + \frac{mU_\theta}{r} - \omega,$$

$$D_\mu = \Lambda_\mu^2 - \frac{2U_\theta}{r^2}\frac{\mathrm{d}}{\mathrm{d}r}(rU_\theta),$$

$$B_\mu = \frac{2mU_\theta}{\Lambda_\mu r^2} - \frac{U_\theta^2}{rc_0^2},$$

B. Change of notations with the other paper

In Mathews *et al.*,[16] a new modified Myers boundary condition is developed to consider the effect of a boundary layer to first order. To make an easy link between the two papers, the change in notations are written below:

$$(\hat{u}, \hat{v}, \hat{w}, \hat{p}) \to (V, W, U, P)$$

References

[1]Ingard, U., "Influence of fluid motion past a plane boundary on sound reflection, absorption, and transmission," *The Journal of the Acoustical Society of America*, Vol. 31, No. 7, 1959, pp. 1035–1036.

[2]Eversman, W. and Beckemeyer, R. J., "Transmission of sound in ducts with thin shear layers—convergence to the uniform flow case," *The Journal of the Acoustical Society of America*, Vol. 52, No. 1B, 1972, pp. 216–220.

[3]Myers, M. K., "On the acoustic boundary condition in the presence of flow," *J. Sound Vib.*, Vol. 71, No. 3, 1980, pp. 429–434.

[4]Brambley, E. J., "Fundamental problems with the model of uniform flow over acoustic linings," *J. Sound Vib.*, Vol. 322, No. 4, 2009, pp. 1026–1037.

[5]Renou, Y. and Aurégan, Y., "On a modified Myers boundary condition to match lined wall impedance deduced from several experimental methods in presence of a grazing flow," *16th AIAA/CEAS Aeroacoustics Conference, Stockholm, Sweden*, No. AIAA Paper 2010-3945, 2010.

[6]Brambley, E. J., "Well-posed boundary condition for acoustic liners in straight ducts with flow," *AIAA journal*, Vol. 49, No. 6, 2011, pp. 1272–1282.

[7]Rienstra, S. W. and Darau, M., "Boundary-layer thickness effects of the hydrodynamic instability along an impedance wall," *J. Fluid Mech.*, Vol. 671, 2011, pp. 559–573.

[8]Gabard, G., "A comparison of impedance boundary conditions for flow acoustics," *J. Sound Vib.*, Vol. 332, No. 4, 2013, pp. 714–724.

[9]Khamis, D. and Brambley, E. J., "Acoustic boundary conditions at an impedance lining in inviscid shear flow," *Journal of Fluid Mechanics*, Vol. 796, 2016, pp. 386–416.

[10]Guan, Y., Luo, K. H., and Wang, T. Q., "Sound transmission in a lined annular duct with mean swirling flow," *ASME 2008 Noise Control and Acoustics Division Conference*, American Society of Mechanical Engineers, 2008, pp. 135–144.

[11]Posson, H. and Peake, N., "The acoustic analogy in an annular duct with swirling mean flow," *J. Fluid Mech.*, Vol. 726, 2013, pp. 439–475.

[12]Posson, N. and Peake, N., "Swirling mean flow effect on fan-trailing edge broadband noise in a lined annular duct," *19^{th} AIAA/CEAS Aeroacoustics Conference and Exhibit, Berlin, Germany*, No. AIAA Paper 2013-2150, 2013.

[13]Mathews, J. R. and Peake, N., "The acoustic Green's function for swirling flow in a lined duct," *Journal of Sound and Vibration*, Vol. 395, 2017, pp. 294–316.

[14]Maldonado, A. L. P., Astley, R. J., Coupland, J., Gabard, G., and Sutliff, D., "Sound Propagation in Lined Annular Ducts with Mean Swirling Flow," *21st AIAA/CEAS Aeroacoustics Conference*, 2015, p. 2522.

[15]Myers, M. and Chuangt, S., "Uniform asymptotic approximations for duct acoustic modes in a thin boundary-layer flow," *AIAA journal*, Vol. 22, No. 9, 1984, pp. 1234–1241.

[16]Mathews, J. R., Masson, V., Moreau, S., and Posson, H., "The modified Myers boundary condition for swirling flow," *23rd AIAA/CEAS Aeroacoustics Conference*, 2017.

[17]Khorrami, R., Malik, M. R., and Ash, R. L., "Application of Spectral Collocation Techniques to the Stability of Swirling Flows," *Journal of Computational Physics*, Vol. 81, No. 1, 1989, pp. 206–229.

[18]Gabard, G., "Boundary layer effects on liners for aircraft engines," *Journal of Sound and Vibration*, Vol. 381, 2016, pp. 30–47.

[19]Hughes, C., Jeracki, R., Woodward, R., and Miller, C., "Fan noise source diagnostic test-rotor alone aerodynamic performance results," *8th AIAA/CEAS Aeroacoustics Conference & Exhibit*, 2002, p. 2426.

[20]Woodward, R., Hughes, C., Jeracki, R., and Miller, C., "Fan Noise Source Diagnostic Test–Far-field Acoustic Results," *8th AIAA/CEAS Aeroacoustics Conference & Exhibit*, 2002, p. 2427.

[21]Masson, V., Posson, H., Sanjose, M., Moreau, S., and Roger, M., "Fan-OGV interaction broadband noise prediction in a rigid annular duct with swirling and sheared mean flow," *22nd AIAA/CEAS Aeroacoustics Conference*, 2016, p. 2944.

[22]Bouley, S., *Modélisations analytiques du bruit tonal d'interaction rotor/stator par la technique de raccordement modal*, Ph.D. thesis, 2017.

[23]Gabard, G. and Astley, R., "A computational mode-matching approach for sound propagation in three-dimensional ducts with flow," *Journal of Sound and vibration*, Vol. 315, No. 4, 2008, pp. 1103–1124.

[24]Posson, H. and Peake, N., "Acoustic analogy in swirling mean flow applied to predict Rotor trailing-edge noise," *18th AIAA/CEAS Aeroacoustics Conference*, No. AIAA Paper 2012-2267, 2012.

[25]Lidoine, S., *Approches théoriques du problème du rayonnement acoustique par une entrée d'air de turboréacteur: comparaisons entre différentes méthodes analytiques et numériques*, Ph.D. thesis, Ecole centrale de Lyon, 2002.

[26]Golubev, V. V. and Atassi, H. M., "Acoustic–vorticity waves in swirling flows," *J. Sound Vib.*, Vol. 209, No. 2, 1998, pp. 203–222.

[27]Boyd, J. P., *Chebyshev and Fourier Spectral Methods*, DOVER Publications, Inc., second edition ed., 2000.

[28]Redheffer, R., "On a certain linear fractional transformation," *Studies in Applied Mathematics*, Vol. 39, No. 1-4, 1960, pp. 269–286.

[29]Foiaş, C. and Frazho, A. E., "Redheffer products and the lifting of contractions on Hilbert space," *Journal of Operator Theory*, 1984, pp. 193–196.

[30]Oppeneer, M., Rienstra, S. W., and Sijtsma, P., "Efficient Mode Matching Based on Closed-Form Integrals of Pridmore-Brown Modes," *AIAA Journal*, Vol. 54, No. 1, 2015, pp. 266–279.

[31]Myers, M., "An exact energy corollary for homentropic flow," *Journal of Sound and Vibration*, Vol. 109, No. 2, 1986, pp. 277–284.